

## AUTOMATIC CONTROL OF MECHATRONIC SYSTEMS

KURT SCHLACHER\*, ANDREAS KUGI\*\*,

This contribution deals with different concepts of nonlinear control for mechatronic systems. Since most physical systems are nonlinear in nature, it is quite obvious that an improvement in the performance of the closed loop can often be achieved only by means of control techniques that take the essential nonlinearities into consideration. Nevertheless, it can be observed that industry often hesitates to implement these nonlinear controllers, despite all advantages existing from the theoretical point of view. On the basis of three different applications, a PWM-controlled dc-to-dc converter, namely the Čuk-converter, the problem of hydraulic gap control in steel rolling, and the design of smart structures with piezoelectric sensor and actuator layers, we will demonstrate how one can overcome these problems by exploiting the physical structure of the mathematical models of the considered plants.

**Keywords:** mechatronic systems, differential geometry, nonlinear  $H_\infty$ -control, passivity, input/output linearization

### 1. Introduction

This paper presents different concepts of nonlinear control for mechatronic systems, with special emphasis on the practical implementation in an industrial environment. Differential geometry and differential algebra will serve as a common mathematical basis for the controller design problem whilst the concepts of passivity and dissipativity will be used to take the physical nature of the to-be-controlled plants into account.

It turns out that in industrial applications large potential for improving the product quality and increasing the efficiency lies in the automation system and the control techniques used. Since most physical systems are nonlinear in nature, it is quite obvious that an improvement in the performance of the closed loop can often be achieved only by means of control techniques that take the essential nonlinearities into consideration. Moreover, the increasing availability of low cost digital signal processors and the use of symbolic computation guarantee the applicability of the proposed nonlinear control strategies. Nevertheless, it can be observed that industry often hesitates to

---

\* Christian Doppler Laboratory for Automatic Control of Mechatronic Systems in Steel Industries, Altenbergerstr. 69, 4040–Linz, Austria,  
e-mail: [schlacher@mechatronik.uni-linz.ac.at](mailto:schlacher@mechatronik.uni-linz.ac.at)

\*\* Department of Automatic Control and Control Systems Technology, Johannes Kepler University of Linz, Altenbergerstr. 69, 4040–Linz, Austria, e-mail: [kugi@mechatronik.uni-linz.ac.at](mailto:kugi@mechatronik.uni-linz.ac.at)

implement these nonlinear controllers, despite all advantages existing from the theoretical point of view. There are several reasons for that, but they follow mainly from the fact that a straightforward application of nonlinear control methods produces satisfying results only in an idealized simulation environment. However, in the industrial reality one has to cope with several restrictions, e.g., only some state variables are measurable, signals are corrupted by nonnegligible transducer and quantization noise, sensors and actuators have a limited accuracy, some parameters are known only inaccurately or are slowly varying due to, e.g., aging processes, and, last but not least, the controllers can be implemented only on a hardware platform with limited sampling time. To our knowledge, a systematic approach to solving all these problems is not available and, of course, we do not intend to present a general solution in this paper. But on the basis of different applications, we will demonstrate how these restrictions can be tackled.

We present the controller design for the Ćuk-converter, a special dc-to-dc converter, in the first example. This example demonstrates a typical mechatronic design. The electrical circuit is kept as simple as possible, which causes some inappropriate behavior of the device. Therefore, one tries to eliminate these shortcomings by the improvement of the controller. As a real-world hydro-mechanical application we will develop the position/force control of a four-high mill stand in a cold rolling mill with the hydraulic adjustment system acting on the upper backup roll. Although here the design problem looks quite simple, the industrial environment corrupts the signals with noise such that the state is available by measurement in principle, but one can use only a subset of the signals for the feedback law.

Apart from the demands on the controller design due to the implementation in an industrial environment, a second feature, mainly stimulated by the philosophy of mechatronics, will be presented. Here, we propose to leave the classical way of a separation between the constructional and the controller design. We will rather regard the design of the actuators and sensors as part of the control loop synthesis. With this, we gain additional degrees of freedom. Furthermore, the right choice of sensors and actuators can often drastically simplify the control task. By means of piezoelectric smart structures we will demonstrate the potential and the feasibility of this proposed integrated design.

Throughout this paper, we consider several systems of ordinary and partial differential equations. To avoid additional technical problems, we assume that all functions are smooth or either continuously differentiable as many times as needed. Roughly speaking, we are more interested in an approach that allows us to implement the derived equations in a computer algebra program than in functional analysis arguments. To avoid long and messy formulas, we use the abbreviation  $\sum_{i=1}^n a_i b^i = a^i b_i = a_i b^i$  for any vector or tensor under consideration, whenever the range of the index  $i$  is clear.

## 2. Ćuk-Converter

Dc-to-dc converters are often used as interfaces between dc systems of different voltage levels in regulated power supplies for electronic equipment and in dc-motor drive ap-

plications (Kassakian *et al.*, 1992; Mohan *et al.*, 1989). By means of feedback control, the average dc-output voltage of the dc-to-dc converter must be controlled to a desired operating level and the dc-output must be kept at this level, if there are any variations in the load or fluctuations in the input voltage. In the so-called high-frequency switch-mode converters, the average output voltage is controlled by adjusting the on- and off-durations of a semiconductor device switching at a rate that is fast compared with the changes in the input and output signals. In the PWM (Pulse-Width-Modulation) case this switching frequency is constant and here the ratio of the on-duration of the switch to the fixed switching time period, also termed the switch duty ratio, is used for controlling the system.

Figure 1 shows the circuit scheme of the Ćuk-converter with the supply voltage  $U_{dc}$ , the internal resistances  $R_1$ ,  $R_2$  of the inductors  $L_1$ ,  $L_2$ , the capacitors  $C_1$ ,  $C_2$ , and the load conductance  $G_2$ . Variations in the load will be considered in the sense

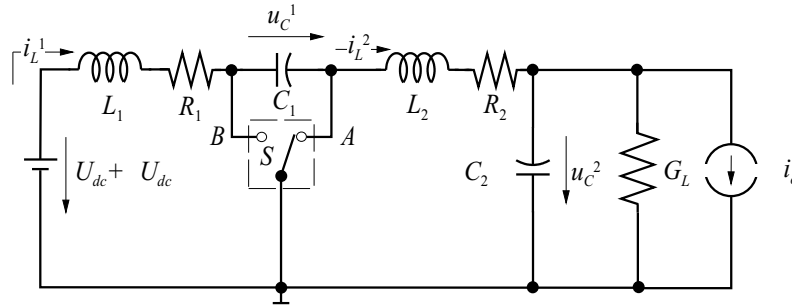


Fig. 1. Circuit scheme of the Ćuk-converter.

of a Norton equivalent circuit (Kassakian *et al.*, 1992) in the form of changes in the output current  $\Delta i_o$ , and fluctuations in the input voltage will be denoted by  $\Delta U_{dc}$ . The switch  $S$  is assumed to have ideal characteristics, which means no losses and zero turn-on and turn-off times. The coordinates  $x^T = [i_L^1, u_C^1, i_L^2, u_C^2]$  (see Fig. 1) form a chart of the network and we can derive the network equations for the switch  $S$  in position  $A$ :

$$\begin{aligned}
 L_1 \frac{d}{dt} i_L^1 &= -R_1 i_L^1 - u_C^1 + U_{dc} + \Delta U_{dc}, \\
 C_1 \frac{d}{dt} u_C^1 &= i_L^1, \\
 L_2 \frac{d}{dt} i_L^2 &= -i_L^2 R_2 - u_C^2, \\
 C_2 \frac{d}{dt} u_C^2 &= i_L^2 - G_2 u_C^2 - \Delta i_o,
 \end{aligned} \tag{1}$$

and in position  $B$ :

$$\begin{aligned}
L_1 \frac{d}{dt} i_L^1 &= -R_1 i_L^1 + U_{dc} + \Delta U_{dc}, \\
C_1 \frac{d}{dt} u_C^1 &= i_L^2, \\
L_2 \frac{d}{dt} i_L^2 &= -u_C^1 - i_L^2 R_2 - u_C^2, \\
C_2 \frac{d}{dt} u_C^2 &= i_L^2 - G_2 u_C^2 - \Delta i_o.
\end{aligned} \tag{2}$$

The Ćuk-converter belongs to the class of pulse-width-controlled networks. Since we choose the nonlinear  $H_\infty$ -approach to the controller design, we start with a short introduction to PWM controlled networks and repeat some results of the nonlinear  $H_\infty$ -design with full information. Finally, we finish this part with a description of the experimental setup and the experimental results.

### 2.1. PWM Controlled Networks

A PWM controlled electrical network like the Ćuk-converter with one switch  $S$  (see Fig. 1) is described by two systems of differential equations in the form

$$\begin{aligned}
\frac{d}{dt} x &= a_A(x), \quad t \in (iT, (i+d_A)T], \quad S \text{ in } A, \\
\frac{d}{dt} x &= a_B(x), \quad t \in ((i+d_A)T, (i+1)T], \quad S \text{ in } B
\end{aligned} \tag{3}$$

for  $i = 0, 1, \dots$  with smooth vector fields  $a_A$ ,  $a_B$  and  $d_A + d_B = 1$ . Here,  $d_B$ ,  $0 \leq d_B \leq 1$  denotes the so-called duty ratio, which specifies the ratio of the duration of the switch  $S$  in position  $B$  to the fixed modulation period  $T$ . Let  $e^{a_A t}(x)$  and  $e^{a_B t}(x)$  denote the flows of the network for the switch  $S$  in positions  $A$  and  $B$ , respectively. Then a solution  $X(t)$  of the network fulfills the relation

$$X((i+1)T) = e^{a_B T d_B} \circ e^{a_A T d_A} (X(iT)) \tag{4}$$

for  $t = iT$ ,  $i = 0, 1, \dots$ . The average model (see, e.g., Kassakian *et al.*, 1992; Sira Ramrez, 1989) of the PWM controlled network

$$\frac{d}{dt} x_a = a_A(x_a) + d_B(a_B(x_a) - a_A(x_a)) \tag{5}$$

is nothing else than the first-order approximation of  $X$  by  $X_a$  and

$$\frac{d}{dt} X_a(iT) = \lim_{T \rightarrow 0} \partial_T e^{a_B T d_B} \circ e^{a_A T(1-d_B)} (X_a(iT)) \tag{6}$$

for  $iT = t$ . This follows directly from the Campbell-Baker-Hausdorff formula (Sastry, 1999)

$$e^{a_B T d_B} \circ e^{a_A T d_A} = e^{(a_B d_B + a_A d_A)T + \frac{1}{2}[a_B, a_A]d_A d_B T^2 + \dots}. \tag{7}$$

Note that the same symbol  $x$  is used here for (3) and its approximation (5). Furthermore, the associated average model (5) is bilinear in the case of linear vector fields  $a_A$  and  $a_B$ .

## 2.2. Nonlinear $H_\infty$ -Design for AI-Systems

The system under consideration is described by the model

$$\begin{aligned} \frac{d}{dt}x^i &= a^i(x) + b_\alpha^i(x)u^\alpha + k_\beta^i(x)d^\beta, \\ y^\gamma &= c^\gamma(x), \end{aligned} \quad (8)$$

with the state  $(x^i) \in \mathcal{U}(0) \subset \mathbb{R}^n$ ,  $i = 1, \dots, n$ , where  $\mathcal{U}(0) \subset \mathbb{R}^n$  is an open neighborhood of the origin, with the control input  $(u^\alpha) \in \mathbb{R}^m$ ,  $\alpha = 1, \dots, m$ , the disturbance  $(d^\beta) \in \mathbb{R}^{m'}$ ,  $\beta = 1, \dots, m'$ , and the output  $(y^\gamma) \in \mathbb{R}^l$ ,  $\gamma = 1, \dots, l$ . We assume for the free system that the origin is an equilibrium and that the set  $\{x \in \mathcal{U} \mid y^\gamma = 0\}$  does not determine an invariant manifold of (8). Let  $\|\cdot\|$  denote the Euclidean norm. The goal of the nonlinear  $H_\infty$ -design is to find a control law

$$u = u(x), \quad u(0) = 0, \quad (9)$$

such that the objective function

$$J = \sup_{T \in [0, \infty)} \inf_{u \in L_2^m[0, T]} \sup_{d \in L_2^{m'}[0, T]} \int_0^T l \, dt \quad (10)$$

with

$$2l(x, u, d) = \|y\|^2 + \|u\|^2 - \gamma \|d\|^2 \quad (11)$$

is minimized with respect to  $u$  and maximized with respect to  $d$ , where  $\gamma > 0$  must be chosen such that the problem is solvable. In a second step, one can try also to minimize  $\gamma$ .

One can show (see, e.g., Isidori and Astolfi, 1992; Knobloch *et al.*, 1993; van der Schaft, 1993; 2000) that the nonlinear  $H_\infty$ -design problem can be converted to the problem of determining a positive definite solution  $V(x)$  of the Hamilton-Jacobi-Bellman-Isaacs-equality

$$\min_u \max_d (\partial_i V (a^i + b_\alpha^i u^\alpha + k_\beta^i d^\beta) + l) = 0 \quad (12)$$

or HJBIE for short. Assuming that such a solution exists, we derive

$$\tilde{u}^\alpha = -b_\alpha^i \partial_i V, \quad \gamma \tilde{d}^\beta = k_\beta^i \partial_i V \quad (13)$$

with optimal choices  $\tilde{u}$ ,  $\tilde{d}$  of  $u$ ,  $d$ . Inserting the optimal choice  $d = \tilde{d}$  of (13) into (11), we can rewrite (12) in the form

$$\min_u \left( 2\partial_i V (a^i + b_\alpha^i u^\alpha) + \|u\|^2 + \|y\|^2 \right) = -\gamma \|\tilde{d}\|^2. \quad (14)$$

Therefore, a positive definite solution  $V(x)$  of (12) is also a Lyapunov function of the closed loop, since  $\|y\|^2$  is a positive semi-definite function of  $x$ . Asymptotic stability follows from the assumption that the set  $\{x \in \mathcal{U} \mid y^\gamma = 0\}$  does not determine an invariant manifold of the free system.

Unfortunately, it is a well-known fact that neither the HJBie (12) nor the corresponding set of Hamiltonian equations can be solved easily. But sometimes it is possible to find a positive definite solution  $V(x)$  of the HJBI-inequality

$$2\partial_i V a^i + \|y\|^2 - \|\tilde{u}\|^2 + \gamma\|\tilde{d}\|^2 \leq 0 \quad (15)$$

and the optimal choice  $u = \tilde{u}$ ,  $d = \tilde{d}$  of (13). Of course, this approach leads to suboptimal solutions only. Furthermore, it is worth mentioning that one gets the nonlinear  $H_2$ -design for the limit  $\gamma \rightarrow \infty$  in a straightforward manner.

### 2.3. Mathematical Model

The average model of the Čuk-converter follows directly from the preceding two subsections in the form

$$\frac{d}{dt}x^i = \left( A_0^{ij} + A_1^{ij} d_B - S^{ij} \right) \partial_j V + B_\alpha^i d^\alpha \quad (16)$$

with

$$[x^i] = \begin{bmatrix} i_L^1 \\ u_C^1 \\ i_L^2 \\ u_C^2 \end{bmatrix}, \quad [d^\alpha] = \begin{bmatrix} U_{dc} + \Delta U_{dc} \\ \Delta i_o \end{bmatrix} \quad (17)$$

for  $i, j = 1, \dots, 4$ ,  $\alpha = 1, 2$ , with the two skew-symmetric matrices  $A_0$ ,  $A_1$ ,

$$[A_0^{ij}] = \begin{bmatrix} 0 & \frac{-1}{L_1 C_1} & 0 & 0 \\ \frac{1}{L_1 C_1} & 0 & 0 & 0 \\ 0 & 0 & 0 & \frac{-1}{L_2 C_2} \\ 0 & 0 & \frac{1}{L_2 C_2} & 0 \end{bmatrix}, \quad (18)$$

$$[A_1^{ij}] = \begin{bmatrix} 0 & \frac{1}{L_1 C_1} & 0 & 0 \\ \frac{-1}{L_1 C_1} & 0 & \frac{1}{L_2 C_1} & 0 \\ 0 & \frac{-1}{L_2 C_1} & 0 & 0 \\ 0 & 0 & 0 & 0 \end{bmatrix},$$

the symmetric matrix

$$[S^{ij}] = \begin{bmatrix} \frac{R_1}{L_1^2} & 0 & 0 & 0 \\ 0 & 0 & 0 & 0 \\ 0 & 0 & \frac{R_2}{L_2^2} & 0 \\ 0 & 0 & 0 & \frac{G_2}{C_2^2} \end{bmatrix}, \quad (19)$$

the input matrix

$$B = \begin{bmatrix} \frac{1}{L_1} & 0 \\ 0 & 0 \\ 0 & 0 \\ 0 & -\frac{1}{C_2} \end{bmatrix} \quad (20)$$

and the stored energy function

$$V = \frac{1}{2} \left( L_1 (i_L^1)^2 + C_1 (u_C^1)^2 + L_2 (i_L^2)^2 + C_2 (u_C^2)^2 \right). \quad (21)$$

Let  $\Delta U_{dc} = 0$ ,  $\Delta i_o = 0$  and  $\bar{d}_B$  determine the operating point  $[\bar{i}_L^1, \bar{u}_C^1, \bar{i}_L^2, \bar{u}_C^2]$  of the Ćuk-converter. We shift this operating point to the origin via the simple transformation

$$\begin{aligned} i_L^1 &= \Delta i_L^1 + \bar{i}_L^1, & u_C^1 &= \Delta u_C^1 + \bar{u}_C^1, \\ i_L^2 &= \Delta i_L^2 + \bar{i}_L^2, & u_C^2 &= \Delta u_C^2 + \bar{u}_C^2, \end{aligned} \quad (22)$$

with  $d_B = \Delta d_B + \bar{d}_B$ . In the new coordinates, (16) can be rewritten as

$$\frac{d}{dt} \Delta x^i = A_1^{ij} \partial_j \bar{V} \Delta d_B + B_\alpha^i \Delta d^\alpha + \left( A_0^{ij} + A_1^{ij} \bar{d}_B + A_1^{ij} \Delta d_B - S^{ij} \right) \partial_j \Delta V \quad (23)$$

with

$$[\Delta x^i] = \begin{bmatrix} \Delta i_L^1 \\ \Delta u_C^1 \\ \Delta i_L^2 \\ \Delta u_C^2 \end{bmatrix}, \quad [\Delta d^\alpha] = \begin{bmatrix} \Delta U_{dc} \\ \Delta i_o \end{bmatrix}, \quad \partial_j = \frac{\partial}{\partial \Delta x^j}, \quad (24)$$

$$\bar{V} = V(\bar{x}) + \partial_j V(\bar{x} + \Delta x)|_{\Delta x=0} \Delta x^j, \quad V = \bar{V} + \Delta V \quad (25)$$

and the matrices of (18)–(20) and  $V$  of (21). Note that  $\Delta V$  is a positive definite function of  $\Delta x$  and that the relation

$$\frac{d}{dt} \Delta V = \partial_i \Delta V \left( A_1^{ij} \partial_j \bar{V} \Delta d_B + B_\alpha^i \Delta d^\alpha \right) - S^{ij} \partial_i \Delta V \partial_j \Delta V \quad (26)$$

is satisfied.

#### 2.4. Controller Design for the Ćuk-Converter

The aim of the controller design is, on the one hand, to keep the output voltage  $u_C^2$  very close to an operating level  $\bar{u}_C^2$  in the presence of disturbances  $\Delta i_o$  and/or  $\Delta U_{dc}$  and, on the other hand, to track any reference trajectory in a prescribed family of exogenous inputs  $\Delta u_{C,\text{ref}}^2$  as well as possible. In order to reach these goals, the model (16) is augmented with an integrator-like-system

$$\frac{d}{dt}z = -az + b(u_{C,\text{ref}}^2 - u_C^2). \quad (27)$$

Clearly, (27) describes only a pure integral action for  $a = 0$ . Again, the relations  $z = \bar{z} + \Delta z$ ,  $u_{C,\text{ref}}^2 = \bar{u}_{C,\text{ref}}^2 + \Delta u_{C,\text{ref}}^2$  allow us to rewrite (27) as

$$\frac{d}{dt}\Delta z = -a\Delta z + b(\Delta u_{C,\text{ref}}^2 - \Delta u_C^2). \quad (28)$$

Obviously, we additionally have

$$\begin{aligned} \Delta H &= (\Delta z)^2 / 2, \\ \frac{d}{dt}\Delta H &= -a(\Delta z)^2 + b\Delta z (\Delta u_{C,\text{ref}}^2 - \Delta u_C^2). \end{aligned} \quad (29)$$

Since for a fixed duty ratio the Ćuk-converter can be locally stabilized by an integrator with negative gain, we choose the control law of the form

$$\Delta d_B = -\Delta z + v \quad (30)$$

with a new plant input  $v$ . In the next step  $v$  is designed by means of the nonlinear  $H_\infty$ -controller design to render the closed loop  $L_2$ -stable. Therefore, we introduce the output  $y$  and new inputs  $u$ ,  $d$ ,

$$\begin{aligned} y &= k_y \Delta u_C^2 \\ u &= k_u v \end{aligned}, \quad d = \begin{bmatrix} k_1 \Delta u_{C,\text{ref}}^2 \\ k_2 \Delta U_{dc} \\ k_3 \Delta i_o \end{bmatrix}, \quad (31)$$

with real numbers  $k_u, k_y, k_\beta > 0$ ,  $\beta = 1, 2, 3$ .

The controller design for the system (23), (28), (30) and (31) is based on the HJBI-inequality (15). We choose  $V = \Delta V + \Delta H$  with  $\Delta V$  from (25) and  $\Delta H$  from (29), see (Kugi and Schlacher, 1999). Now, minimization with respect to  $u$  leads to

$$\tilde{u} = -k_u^{-1} \left( \Delta u_C^1 (\bar{i}_L^2 - \bar{i}_L^1) - \bar{u}_C^1 (\Delta i_L^2 - \Delta i_L^1) \right) \quad (32)$$

and maximization with respect to  $d_\beta$  generates the relations

$$\gamma \tilde{d}^1 = k_1^{-1} b \Delta z, \quad \gamma \tilde{d}^2 = k_2^{-1} \Delta i_L^1, \quad \gamma \tilde{d}^3 = -k_3^{-1} \Delta u_C^2. \quad (33)$$

Since the function

$$\frac{d}{dt}V = \frac{d}{dt}\Delta V + \frac{d}{dt}\Delta H \quad (34)$$

with  $d\Delta V/dt$  from (26) and  $d\Delta H/dt$  from (29) is a quadratic form in the variables  $\Delta x^i$  and  $\Delta z$  by construction, one can check the positive definiteness with the Sylvester criterion. A straightforward calculation leads to the inequalities

$$2G_2 > k_y^2, \quad (35)$$

$$2R_1 k_2^2 \gamma > 1, \quad (2G_2 - k_y^2) k_3^2 \gamma > 1 \quad (36)$$

and

$$a \geq \frac{b^2}{2k_1^2 \gamma} + \frac{1}{2} k_u^2 + \frac{1}{2} \frac{\gamma k_3^2 b^2}{(2G_2 - k_y^2) k_3^2 \gamma - 1}. \quad (37)$$

For the nonlinear  $H_2$ -design, or  $\gamma \rightarrow \infty$  in (12), we have to meet only (35) and

$$a \geq \frac{1}{2} k_u^2 + \frac{1}{2} \frac{b^2}{2G_2 - k_y^2}. \quad (38)$$

Summarizing (27), (28), (31) and (32), the control law takes the form

$$\begin{aligned} \frac{d}{dt} \Delta z &= -a \Delta z + b \left( \Delta u_{C,\text{ref}}^2 - \Delta u_C^2 \right) \\ \Delta d_B &= -k_u^{-2} \left( \Delta u_C^1 (\bar{i}_L^2 - \bar{i}_L^1) - \bar{u}_C^1 (\Delta i_L^2 - \Delta i_L^1) \right) - \Delta z \end{aligned} \quad (39)$$

and the corresponding closed loop has an  $L_2$ -gain  $\leq \gamma$  with a lower bound for  $\gamma$  from (36). Furthermore, the control law is linear and can be easily implemented even in the form of an analog circuit. This is sometimes of great interest for low-cost implementation, where digital processors are not available. The parameters  $a$ ,  $b$  and  $k_u$  are used to adjust the performance of the closed loop, where the choice of these parameters results from heuristic considerations (Kugi and Schlacher, 1999).

Apart from the nonlinear  $H_\infty$ -controller design with the objective function (31), various other possible objective functions were taken into account. However, the reason for the proposed choice can be summarized as follows. In this approach the tracking task is actually performed by the integrator-like controller (27) and (28), and the outer-loop nonlinear  $H_\infty$ -controller (32) is designed to render the closed loop system dissipative. In this manner it is also guaranteed that the Ćuk-converter can operate on different operating levels which are not known *a priori*. This was also supposed to be a technological demand on our design. Another successful approach where the integral part is systematically included in the nonlinear  $H_2$ -controller design can be found in (Kugi, 2000).

## 2.5. Experimental Setup

To check the feasibility of the proposed controller, a laboratory model has been set up for performing the experiments of the Ćuk-converter with the parameter values  $L_1 = L_2 = 10.9 \times 10^{-3}$  H,  $R_1 = R_2 = 1.3 \Omega$ ,  $C_1 = 22.0 \times 10^{-6}$  F,  $C_2 = 22.9 \times 10^{-6}$  F and  $U_{\text{dc}} = 12$  V. The capacitor  $C_1$  is located in an external pin base and can also be exchanged due to experimental requirements. The load can be chosen to be either

a resistor with a fixed conductance  $G_L = 1/22.36 \text{ S}$  or via a programmable load simulator, and the load conductance can be set to an arbitrary value in a range  $G_L \leq 1/6.4 \text{ S}$ . The value of the programmable load simulator can be defined by a control voltage  $u_{\text{load}}$ . The switch  $S$  is realized with a standard MOSFET (BUZ11) in combination with the MOSFET-drive-IC SI9910DJ and a Schottky Diode (MBR1060) with a low forward voltage drop. The modulation frequency for the PWM actuator (either IC SG3524 or internal PWM of the DSP-unit) is chosen as 25 kHz in order to keep the total losses in the converter at a minimum. The two inductor currents  $i_L^1$  and  $i_L^2$  are measured by means of  $0.1 \Omega$  shunt resistors and instrumentation amplifier ICs (Burr Brown INA2128/2) with low offset and drift. The capacitor voltages  $u_C^1$  and  $u_C^2$  are also directly measured by means of instrumentation amplifier ICs and all the measurement signals are filtered with 4th-order analog Bessel low-pass filters with a cut-off frequency of 10 kHz. The Ćuk-converter experiment operates together with a DSP-system (dSpace) integrated in a PC running WINDOWS NT which enables us to use the MATLAB/SIMULINK environment to test the controllers. This hard- and software configuration allows the sampling times to be reduced to  $2 \times 10^{-4} \text{ s}$ . For more details concerning the experimental setup the reader is referred to (Kugi, 2000).

For analyzing small-signal dynamics, the Ćuk-converter system (23) is linearized around an operating point  $\bar{x}^T = [\bar{i}_L^1, \bar{u}_C^1, \bar{i}_L^2, \bar{u}_C^2]$ . The symbol  $\delta$  indicates the linearized quantities. We consider the transfer function

$$\delta \hat{u}_C^2 = G(s, \bar{d}_B) \delta \hat{d}_B \quad (40)$$

at an operating point  $\bar{d}_B$  as a function of the Laplace variable  $s$ . The symbol ‘ $\hat{\cdot}$ ’ indicates the corresponding Laplace-transformed quantity. Now, it is possible to calculate the poles and zeros of the transfer function as a function of  $\bar{d}_B$ . For the laboratory model the zeros and poles are depicted in Figs. 2 and 3, respectively, where the square indicates the point  $\bar{d}_B = 0$  and the circles represent the results for  $\bar{d}_B$  in

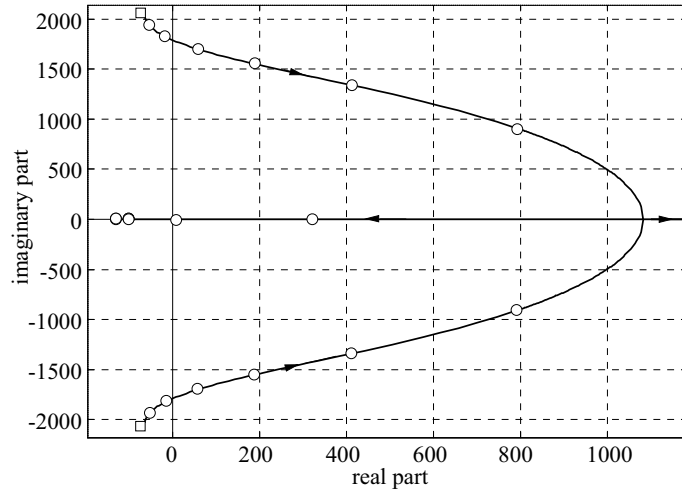


Fig. 2. Zeros of the transfer function  $G(s, \bar{d}_B)$  as a function of the duty ratio  $\bar{d}_B$ .

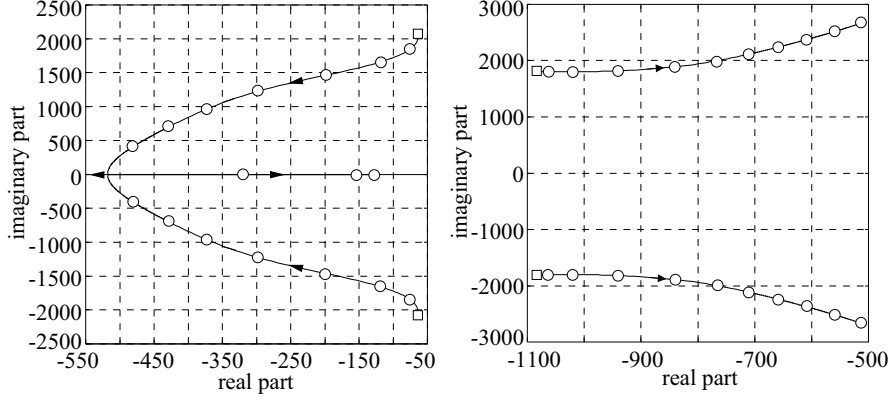


Fig. 3. Poles of the transfer function  $G(s, \bar{d}_B)$  as a function of the duty ratio  $\bar{d}_B$ .

0.1 steps from  $\bar{d}_B = 0$  to  $\bar{d}_B = 1$ . An important feature of the Ćuk-converter is the fact that from  $\bar{d}_B = 0.227$  upwards the zeros of the transfer function lie in the closed right half  $s$ -plane or, in other words, the Ćuk-converter shows a bifurcation of the zero dynamics. This fact can also be seen in Fig. 4, where the measured and simulated transient responses of the nonlinear model for a step input of the duty ratio  $\delta d_B = 0.2\sigma(t - 5 \times 10^{-3})$  for two operating points  $\bar{d}_B = 0$  and  $\bar{d}_B = 0.5$  are illustrated. In the case of  $\bar{d}_B = 0.5$  the step responses of  $i_L^2$  and  $u_C^2$  exhibit a typical non-minimum phase behavior.

## 2.6. Measurement and Simulation Results

For the experimental investigations the operating point of the duty ratio is fixed at  $\bar{d}_B = 0.49$  and hence with  $U_{dc} = 12$  V and  $G_L = 1/22.36$  S we get  $\bar{x}^T = [\bar{i}_L^1, \bar{u}_C^1, \bar{i}_L^2, \bar{u}_C^2] = [0.44, 22.01, -0.45, -10.0]$ . The parameters of the controller (39) are chosen as  $k_u = 10$ ,  $a = 0.001$  and  $b = 8$  and a sampling time of  $3 \times 10^{-4}$  s is used.

Figure 5 shows the simulated and measured output voltage  $u_C^2$  and the corresponding duty ratio  $d_B$  for the reference input

$$\Delta u_{C,\text{ref}}^2 = 8\sigma(t - 0.9 \times 10^{-2}) - 18\sigma(t - 4.9 \times 10^{-2}) + 8\sigma(t - 8.9 \times 10^{-2}) \quad (41)$$

with  $\sigma(t)$  as the unit step.

Figure 6 depicts the simulated and measured transient responses of the output voltage  $u_C^2$  and of the corresponding duty ratio  $d_B$ , when the converter is subjected to a load variation  $G_L = 1/22.36 + \Delta G_L$  with

$$\Delta G_L = \left(\frac{1}{90} - \frac{1}{22.36}\right)\sigma(t - 0.9 \times 10^{-2}) - \left(\frac{1}{90} - \frac{1}{7.5}\right)\sigma(t - 4.9 \times 10^{-2}). \quad (42)$$

One can easily convince oneself that the proposed controller has an excellent tracking and disturbance rejection behavior, and that the duty ratio  $d_B$  remains within the admissible boundaries.

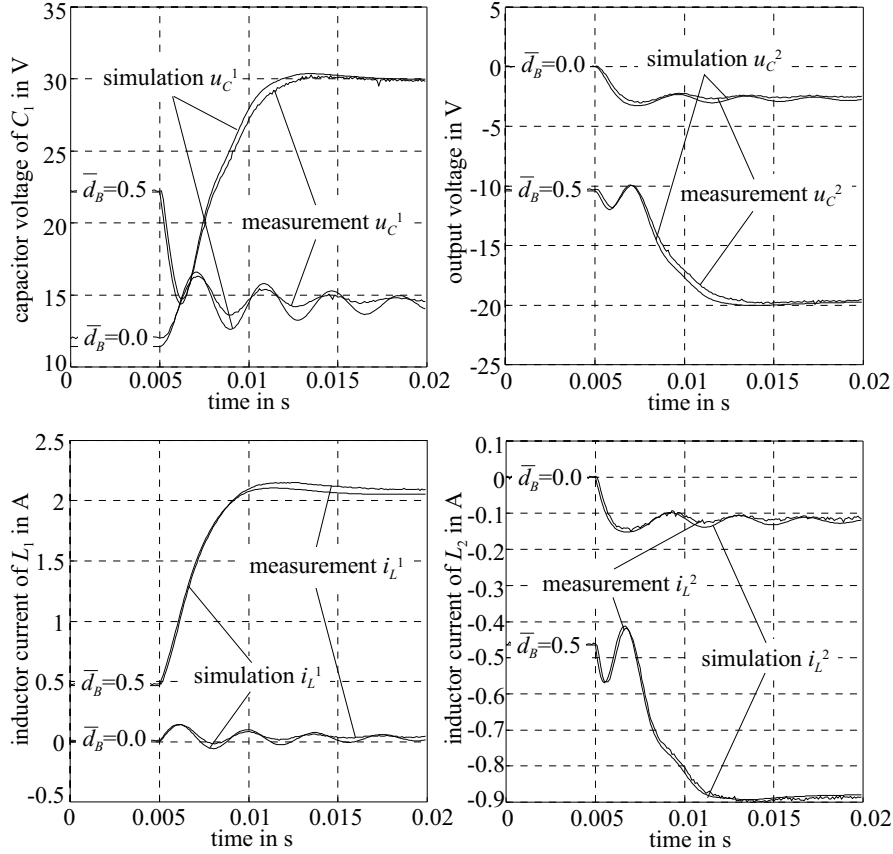


Fig. 4. Step responses at two different operating points  $\bar{d}_B = 0$  and  $\bar{d}_B = 0.5$ .

### 3. Hydraulic Gap Control

In rolling mills, there is a strong tendency to improve the quality of the rolled product, especially concerning the thickness tolerance. Apart from the mechanical equipment, the actuators and sensors, big potential for ensuring good quality lies in the automation system and the employed control techniques. Especially in the case of revamping an existing mill, the mechanical equipment is not always of the state of the art but, nevertheless, the automation system has to satisfy the customers' requirements. Since the time limits for the start-up time of a mill are very short, it is also necessary to test the controllers in advance on a mill simulator in addition to the standard integration tests of the automation system. Here, it is of great importance that the mathematical models of the mill simulator take into account all the essential effects of the dynamic behavior of the mill stand and that they match the real plant as well as possible.

Throughout this section, a position-controlled hydraulic adjustment system is assumed. It is a matter of fact that the hydraulic adjustment system is nonlinear in nature and therefore, in order to guarantee that the closed-loop system has the same

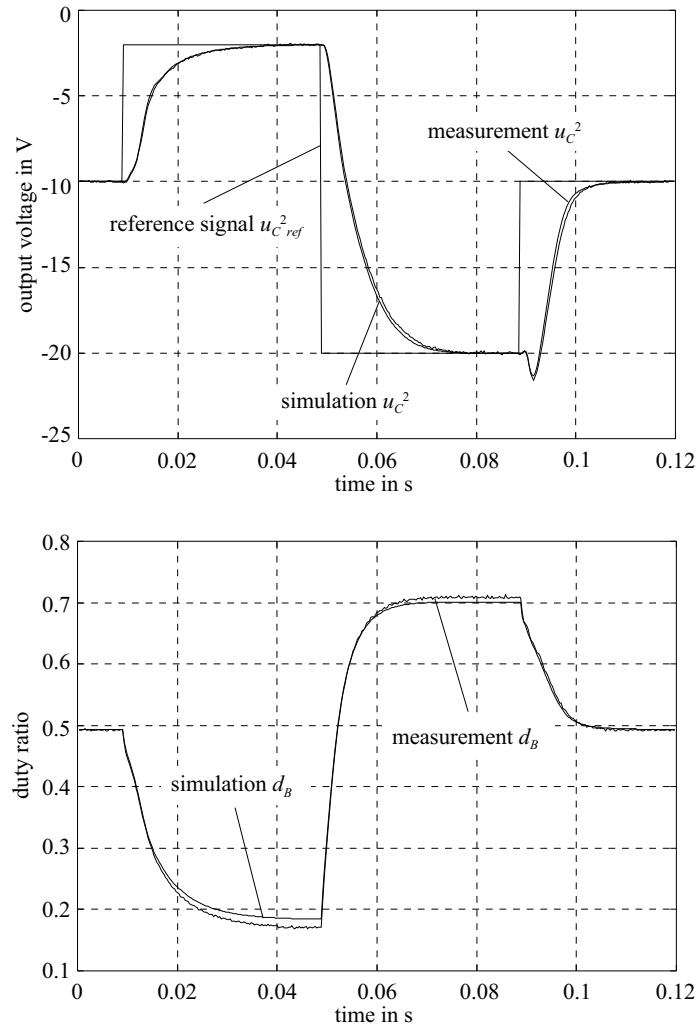


Fig. 5. Measurement and simulation results for the tracking behavior.

dynamic behavior over the operating range, the essential nonlinearities have to be taken into account in the controller design. Furthermore, the control task becomes more difficult because not all quantities are available through measurement, and the measured quantities are corrupted by transducer and quantization noise. Figure 7 presents the schematic diagram of a four-high mill stand with the hydraulic adjustment system acting on the upper backup roll system. Subsequently, we assume with no loss of generality that the hydraulic adjustment system consists of a double acting hydraulic piston controlled by a critical center three-land-four-way spool valve.

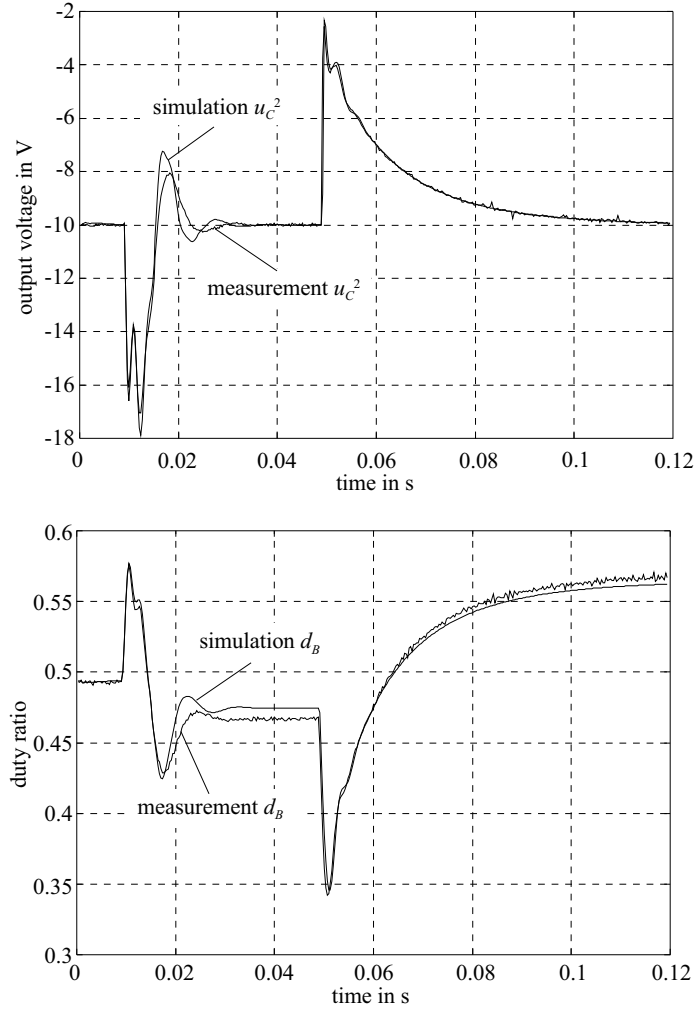


Fig. 6. Measurement and simulation results for the disturbance behavior.

We will use the well-known input/output linearization for the controller design. Therefore, we give a short review of this method, after presenting the mathematical model along with its properties and restrictions for the controller design. Then we continue with the controller design and discuss some simulation results.

### 3.1. Mathematical Model

For the derivation of the mathematical model of the hydraulic piston the following aspects are taken for granted: The servo valves are rigidly connected to a constant pressure pump and the supply pressure remains constant during all possible operations. The temperature of the oil is constant and the oil is supposed to be isotropic.

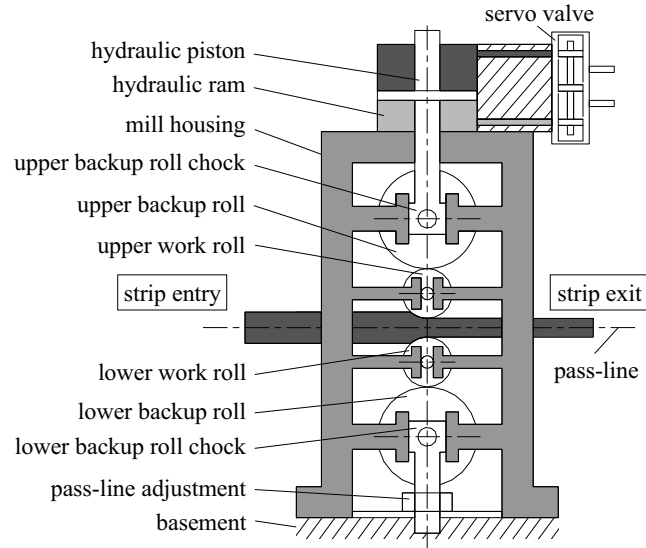


Fig. 7. Schematic diagram of a four-high mill stand.

From the last two properties we may deduce that the mass density of the oil  $\rho_{oil}$  depends only on the pressure  $p$  of the corresponding chamber. Hence from Fig. 8 the continuity equations for the two chambers read as

$$\begin{aligned} \frac{d}{dt} (\rho_{oil}(p^1) (V_0^1 + A_{eff}^1 x_k)) &= \rho_{oil}(p^1) (q^1 - q_{int} - q_{ext}^1), \\ \frac{d}{dt} (\rho_{oil}(p^2) (V_0^2 - A_{eff}^2 x_k)) &= \rho_{oil}(p^2) (q_{int} - q_{ext}^2 - q^2), \end{aligned} \quad (43)$$

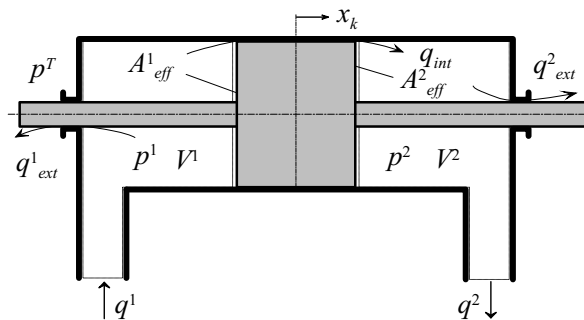


Fig. 8. Double-ended, double-acting hydraulic ram.

with volumes  $V_0^1$  and  $V_0^2$  of the forward and the return chamber for  $x_k = 0$ , respectively, effective piston areas  $A_{\text{eff}}^1$  and  $A_{\text{eff}}^2$ , the displacement of the piston  $x_k$ , the flow from the valve to the forward chamber  $q^1$ , the flow from the return chamber to the valve  $q^2$ , the internal leakage flow  $q_{\text{int}}$ , and the external leakage flows  $q_{\text{ext}}^1$  and  $q_{\text{ext}}^2$ . Inserting the relation for the isothermal bulk modulus of oil  $E_{\text{oil}}$  (Merritt, 1967)

$$\frac{E_{\text{oil}} \partial \rho_{\text{oil}}}{\partial p} = \rho_{\text{oil}}(p) \quad (44)$$

in (43), and using the fact that the leakage flows are laminar, we obtain

$$\begin{aligned} (V_0^1 + A_{\text{eff}}^1 x_k) \frac{d}{dt} p^1 &= E_{\text{oil}} (q^1 - A_{\text{eff}}^1 v_k - C_{\text{int}} (p^1 - p^2) - C_{\text{ext}}^1 p^1), \\ (V_0^2 - A_{\text{eff}}^2 x_k) \frac{d}{dt} p^2 &= E_{\text{oil}} (-q^2 + A_{\text{eff}}^2 v_k + C_{\text{int}} (p^1 - p^2) - C_{\text{ext}}^2 p^2), \end{aligned} \quad (45)$$

with  $v_k = dx_k/dt$  and the leakage coefficients  $C_{\text{int}}$ ,  $C_{\text{ext}}^1$  and  $C_{\text{ext}}^2$ . The flows  $q^1$ ,  $q^2$  from and to the valve can be calculated by

$$\begin{aligned} q^1 &= K_v^1 \sqrt{p^S - p^1} \text{sg}(x_v) - K_v^2 \sqrt{p^1 - p^T} \text{sg}(-x_v), \\ q^2 &= K_v^2 \sqrt{p^2 - p^T} \text{sg}(x_v) - K_v^1 \sqrt{p^S - p^2} \text{sg}(-x_v), \end{aligned} \quad (46)$$

with the supply and the tank pressure  $p^S$  and  $p^T$ , respectively, the valve displacement  $x_v$ , the function  $\text{sg}(x) = x$  for  $x > 0$ , and  $\text{sg}(x) = 0$  for  $x \leq 0$  and the coefficients  $K_v^i = C_d A_v^i \sqrt{2/\rho_{\text{oil}}}$ ,  $i = 1, 2$ , where  $A_v^i$  is the orifice area and  $C_d$  the discharge coefficient (see, e.g., Merritt, 1967). In this description the leakage characteristic and the friction of the valve have been neglected, although they are included in the simulation model, and it is assumed that the valve is closed-center with zero effective lap. Since the dynamics of the spool valve are much faster than the other components of the system, we will neglect them and consider the valve displacement  $x_v$  as the plant input to the system.

For testing the controllers on the mill simulator, the mill stand is modeled in the form of discrete masses, springs and dampers. One has to take into account the roll force  $F_r$  as well as the friction forces between the work and the backup roll chocks and the mill housing, see (Kugi, 2000). The deformation process of the strip is considered in the form of static roll force models for cold or hot rolling. As long as no spatial distribution of the roll load and no dynamic effects of the deformation process are taken into account, we can reduce the deformation models to systems of implicit nonlinear equations of the form

$$f_{\text{roll}}(F_r, h_{\text{ex}}, h_{\text{en}}, \sigma_{\text{ex}}, \sigma_{\text{en}}, \omega_{\text{roll}}, T_{\text{st}}, \sigma_F) = 0$$

with exit and entry thicknesses  $h_{\text{ex}}$  and  $h_{\text{en}}$ , specific exit and entry tensions  $\sigma_{\text{ex}}$  and  $\sigma_{\text{en}}$ , the angular velocity of the work or backup roll  $\omega_{\text{roll}}$ , the strip temperature  $T_{\text{st}}$ , and the yield stress  $\sigma_F$ . However, the setting up of these deformation models consists in solving various differential and integral equations as well as the definitions of many parameters, e.g., the friction coefficient between the rolls and the strip (see, e.g., (Hensel and Spittel, 1990) or more recently, (Fleck *et al.*, 1992) and the references cited therein).

### 3.2. Properties and Restrictions of the Plant

There are certain features of the plant that must be taken into account for the controller design and must be included in the mill simulator in order to obtain a controller that can be successfully implemented in the plant.

- (a) Only the pressures  $p^1$  and  $p^2$  of the two chambers of the hydraulic cylinder and the displacement of the hydraulic piston  $x_k$  are directly measurable.
- (b) The measurement signals  $p^1$ ,  $p^2$  and  $x_k$  are corrupted by transducer noise and nonnegligible quantization noise.
- (c) Due to different leakage flows of the valve, the pressures  $p^1$  and  $p^2$  in the forward and return chambers may have a considerable offset value from symmetrical pressure conditions. These offset pressures have a dominating influence on the dynamic behavior of the hydraulic system, especially if the piston is near one of the two edges of the cylinder.
- (d) The velocity of the piston  $v_k$  cannot be directly measured and an observer for the velocity, which is based on the position signal, fails due to the transducer and quantization noise. But the velocity-dependent term on the right-hand side of (45) cannot be neglected in the dynamic case. Furthermore, the parameters of the stand model are known rather inaccurately and the roll force  $F_r$ , or at least the roll force deviation from the nominal value, has to be considered as a disturbance on the system. This is also why the controllers based on the knowledge of the state variables of the stand or on an observation of these state variables cannot be used in practice.
- (e) A very important fact for both the commissioning engineer and the maintenance staff is that the dynamics of the hydraulic actuation system can be easily adjusted and that the stability of the closed loop can be guaranteed over the operating range.

### 3.3. Input/Output Linearization with Constraints

Now, the system under consideration is the simple SISO-system

$$\frac{d}{dt}x^i = a^i(x) + b^i(x)u \quad (47)$$

with the state  $(x^i) \in \mathcal{U}(0) \subset \mathbb{R}^n$ ,  $i = 1, \dots, n$ , where  $\mathcal{U}(0)$  is an open neighborhood of the origin, and with the single control input  $u \in \mathbb{R}$ .

Let us recall shortly the input/output linearization approach (e.g., see, Isidori, 1996; Nijmeijer and van der Schaft, 1991). We assume that there exists an output  $y \in \mathbb{R}$  with  $y = c(x)$  such that the relations

$$(ba^{k-2}(c))(x) = 0, \quad ((ba^{k-1})(c))(x) \neq 0 \quad (48)$$

are met in a neighborhood of a point  $x$  for  $k \geq 1$ . Here  $a(c) = a^i \partial_i c$  denotes the Lie-derivative of a function  $c$  along the vector field  $a$ . Furthermore, we use the

abbreviations  $a^{k+1}(c) = a(a^k(c))$ ,  $a^0(c) = c$ ,  $k \geq 1$ , as well as  $ba(c) = b(a(c))$ . One can show that there exists a state-transformation

$$z^i = w^i(x) \quad (49)$$

such that (47) takes the form

$$\begin{aligned} \dot{z}^j &= z^{j+1}, \\ \dot{z}^k &= (a^k(c))(w^{-1}(z)) + (ba^{k-1}(c))(w^{-1}(z))u, \\ \dot{z}^l &= f^l(z) \end{aligned} \quad (50)$$

in the new coordinates  $z$  with  $j = 1, \dots, k-1$ ,  $l = k+1, \dots, n$  and  $z^j = a^{j-1}(c)$ . Obviously, the input transformation

$$u = \frac{v - a^k(c)}{ba^{k-1}(c)} \quad (51)$$

leads to a linear behavior between the new input  $v$  and the output  $y = c$  in a neighborhood of  $x$ . Now, we impose the additional constraint that the part  $(z^1, \dots, z^k)$  of (50) is independent of the variable  $x^n$ . From the relations  $\partial_n a^j(c) = 0$ ,  $j = 0, \dots, k$  and (48), we get the additional conditions

$$\begin{aligned} (\text{ad}_a^j \partial_n)(c) &= 0, \quad j = 1, \dots, k, \\ [\text{ad}_a^{k-1} b, \partial_n](c) &= 0. \end{aligned} \quad (52)$$

Here  $[\cdot, \cdot]$  denotes the Lie-bracket  $[a, b] = b(a^i) \partial_i - a(b^i) \partial_i$  and  $\text{ad}_a^k b$  stands for the repeated Lie-bracket with  $\text{ad}_a^0 b = b$ ,  $\text{ad}_a^{k+1} b = [\text{ad}_a^k b, b]$ .

### 3.4. Controller Design

Several different control strategies have been presented in the literature for the nonlinear control of hydraulic systems. Nevertheless, in industry one will often find the classical approach of a  $P$  controller, sometimes with a static servo compensation. One of the main reasons behind this situation is that many of the proposed nonlinear controllers can neither be implemented in practice, due to the lack of measurements or due to the sensitivity to quantization noise, nor improve the results obtained by the classical approach.

Let us take as a basis for the controller design the continuity equations (45) and assume that the internal and external leakage flows can be neglected when compared with the other flows. Then (45) takes the form

$$\begin{aligned} (V_0^1 + A_{\text{eff}}^1 x_k) \frac{d}{dt} p^1 &= E_{\text{oil}} (q^1 - A_{\text{eff}}^1 v_k), \\ (V_0^2 - A_{\text{eff}}^2 x_k) \frac{d}{dt} p^2 &= E_{\text{oil}} (A_{\text{eff}}^2 v_k - q^2), \end{aligned} \quad (53)$$

with  $q^1$  and  $q^2$  from (46). Furthermore, for the controller design, we neglect the dynamics of the mill stand and then the equation of motion for the piston takes the form

$$\begin{aligned} \frac{d}{dt}x_k &= v_k, \\ m_k \frac{d}{dt}v_k &= F_h - m_k g - d_k v_k - F_d, \end{aligned} \quad (54)$$

where  $F_h = A_{\text{eff}}^1 p^1 - A_{\text{eff}}^2 p^2$  and  $m_k$  denotes the sum of the piston mass and all the masses rigidly connected to the piston,  $d_k$  is the damping coefficient, and  $F_d$  signifies the external force on the piston, which is assumed to be constant but unknown.

Previously we discussed in detail that the control law must not contain the piston velocity  $v_k$ . Therefore, we are looking for a description of (53) where the dependence on  $v_k$  vanishes. This can be achieved by the following state transformation (Kugi *et al.*, 1999b):

$$\begin{aligned} z^1 &= p^1 + E_{\text{oil}} \ln(V_0^1 + A_{\text{eff}}^1 x_k), \\ z^2 &= p^2 + E_{\text{oil}} \ln(V_0^2 - A_{\text{eff}}^2 x_k). \end{aligned} \quad (55)$$

Then (53) can be rewritten as

$$\begin{aligned} \frac{d}{dt}z^1 &= \frac{E_{\text{oil}}}{V_0^1 + A_{\text{eff}}^1 x_k} q^1, \\ \frac{d}{dt}z^2 &= \frac{-E_{\text{oil}}}{V_0^2 - A_{\text{eff}}^2 x_k} q^2. \end{aligned} \quad (56)$$

One can immediately see that  $z^1$  and  $z^2$  remain constant as long as the flows from and to the valve  $q^1$  and  $q^2$  are zero. Clearly, (55) is nothing else than the pressure of the chambers  $p^1$  and  $p^2$  plus the deviation of the pressure due to the change in the chamber volumes. However, assuming that the compressibility of oil  $E_{\text{oil}}$  is constant, we directly obtain (55) by solving (44) with  $\rho_{\text{oil}} = M/V$ , where  $V$  is the considered volume and  $M$  the mass of the oil in this volume. Now, we apply the input/output linearization of (51) to the output function  $y$ ,

$$y = A_{\text{eff}}^1 z^1 - A_{\text{eff}}^2 z^2. \quad (57)$$

From (48) we get  $k = 1$ , and a short calculation shows that we obtain for all operating conditions a linear input/output behavior from the new input  $u$  to  $y$  by applying the input transformation

$$x_v = \left( \frac{A_{\text{eff}}^1 E_{\text{oil}}}{V_0^1 + A_{\text{eff}}^1 x_k} K_v^1 \sqrt{p^S - p^1} + \frac{A_{\text{eff}}^2 E_{\text{oil}}}{V_0^2 - A_{\text{eff}}^2 x_k} K_v^2 \sqrt{p^2 - p^T} \right)^{-1} u \quad (58)$$

for  $x_v > 0$  and

$$x_v = - \left( \frac{A_{\text{eff}}^1 E_{\text{oil}}}{V_0^1 + A_{\text{eff}}^1 x_k} K_v^2 \sqrt{p^1 - p^T} + \frac{A_{\text{eff}}^2 E_{\text{oil}}}{V_0^2 - A_{\text{eff}}^2 x_k} K_v^2 \sqrt{p^S - p^2} \right)^{-1} u \quad (59)$$

for  $x_v < 0$ . Thus the system (53) and (54) takes the form

$$\begin{aligned}\frac{d}{dt}z &= u, \\ \frac{d}{dt}x_k &= v_k, \\ m_k \frac{d}{dt}v_k &= z - m_k g - d_k v_k - F_d - f(x_k),\end{aligned}\tag{60}$$

with

$$f(x_k) = E_{\text{oil}} \ln \frac{(V_0^1 + A_{\text{eff}}^1 x_k)^{A_{\text{eff}}^1}}{(V_0^2 - A_{\text{eff}}^2 x_k)^{A_{\text{eff}}^2}}.\tag{61}$$

Obviously, the conditions (52) are met. For the subsequent considerations let us assume without restriction of generality that the hydraulic cylinder is built up symmetrically, i.e.,  $A_{\text{eff}}^1 = A_{\text{eff}}^2 = A_{\text{eff}}$  and  $V_0^1 = V_0^2 = V_0$ . For controlling the position of the hydraulic piston  $x_k$  we use the control law (58), (59) and

$$u = \alpha_1 f(\Delta x_k)\tag{62}$$

with the function  $f$  from (61) and  $\Delta x_k = x_{k,\text{ref}} - x_k$ , where  $x_{k,\text{ref}}$  denotes the reference value of  $x_k$  and  $\alpha_1 > 0$ , see (Kugi, 2000). Now, if we formulate (60) with (62) around a stationary point, then the closed-loop system written in deviations  $\Delta$  from this stationary point reads as

$$\begin{aligned}\frac{d}{dt}\Delta z &= -\alpha_1 f(\Delta x_k), \\ \frac{d}{dt}\Delta x_k &= \Delta v_k, \\ m_k \frac{d}{dt}\Delta v_k &= \Delta z - d_k \Delta v_k - f(\Delta x_k),\end{aligned}\tag{63}$$

with the nonlinear function

$$f(\Delta x_k) = E_{\text{oil}} A_{\text{eff}} \ln \left( \frac{V_0 - A_{\text{eff}} x_{k,\text{ref}}}{V_0 - A_{\text{eff}} (\Delta x_k + x_{k,\text{ref}})} \frac{V_0 + A_{\text{eff}} (\Delta x_k + x_{k,\text{ref}})}{V_0 + A_{\text{eff}} x_{k,\text{ref}}} \right).\tag{64}$$

The key observation here is that the static nonlinearity  $f(\Delta x_k)$  satisfies the sector condition

$$0 \leq c_k \Delta x_k^2 \leq f(\Delta x_k) \Delta x_k < \infty\tag{65}$$

with  $c_k = 2E_{\text{oil}} A_{\text{eff}}^2 / V_0$  for  $\Delta x_{k,\text{min}} < \Delta x_k < \Delta x_{k,\text{max}}$ ,  $\Delta x_{k,\text{min}} = -V_0 / A_{\text{eff}} - x_{k,\text{ref}}$  and  $\Delta x_{k,\text{max}} = V_0 / A_{\text{eff}} - x_{k,\text{ref}}$ . Now, the mathematical model (63) and (64) can be represented as a feedback interconnection of a reachable and observable linear subsystem with the transfer function

$$G(s) = \frac{s + \alpha_1}{m_k s^3 + d_k s^2 + c_k s + c_k \alpha_1}\tag{66}$$

and the static nonlinearity

$$\psi(\Delta x_k) = f(\Delta x_k) - c_k \Delta x_k \quad (67)$$

with  $f(\Delta x_k)$  from (64). By means of the Popov criterion (see, e.g., Khalil, 1992), it can be shown that the closed loop is absolutely stable if the condition

$$0 < \alpha_1 < \min\left(\frac{d_k}{m_k}, \frac{c_k}{d_k}\right) \quad (68)$$

is satisfied (Kugi, 2000). At first sight, this result seems to be local because the sector condition (65) holds only in the finite domain  $\Delta x_{k,\min} < \Delta x_k < \Delta x_{k,\max}$ . But it can be shown that the set  $\Omega = \{\Delta z, \Delta x, \Delta v \in \mathbb{R} \mid \Delta x_{k,\min} < \Delta x_k < \Delta x_{k,\max}\}$  is positively invariant, i.e., every trajectory starting in  $\Omega$  remains for all future time moments in  $\Omega$  (Kugi, 2000). Therefore we can deduce that every stationary point defined by  $x_{k,\text{ref}}$  is globally asymptotically stable in  $\Omega$ .

### 3.5. Simulation Results

We consider three different operating positions of the hydraulic piston, namely when the piston is in the middle of the cylinder (Case A), when the piston is in relation to the length of the cylinder 5% from the top edge of the cylinder (Case B), and when the piston is in relation to the length of the cylinder 5% from the bottom edge of the cylinder (Case C). The simulation results for the position control with the reference input

$$x_{k,\text{ref}} = 50 \times 10^{-6} (2\sigma(t - 0.1) - \sigma(t - 0.3)) \quad (69)$$

are presented in Fig. 9. Here  $\Delta x_k$  denotes the displacement deviation of the hydraulic piston from the nominal operating position,  $x_v$  is the corresponding spool valve position, and  $\sigma$  stand for the unit step. For this simulation an operating point for the roll force of 5.4 MN, an offset pressure from symmetrical pressure conditions of 50 bar, and a quantization of the position of the hydraulic piston of  $5 \mu\text{m}$  were assumed. As can be seen from Fig. 9, the most important feature of this controller is that the dynamic behavior of the hydraulic piston remains the same over the operating range. Furthermore, it can be implemented by using only measurable quantities and various simulation studies and field tests prove that it is robust against transducer and quantization noise and varying leakage parameters. It is worth mentioning that the only restriction for the state transformation (55) is the fact that the compressibility of oil  $E_{\text{oil}}$  is constant but it does not rely on its specific value.

## 4. Smart Structures

Smart structures based on piezoelectricity represent an important new group of actuators and sensors for active vibration control of mechanical systems. In contrast to conventional techniques, this technology allows us to construct spatially-distributed devices (see, e.g., Tzou, 1992). This fact requires special control techniques to improve the dynamical behavior of this kind of smart structures (see, e.g., Kugi *et al.*,

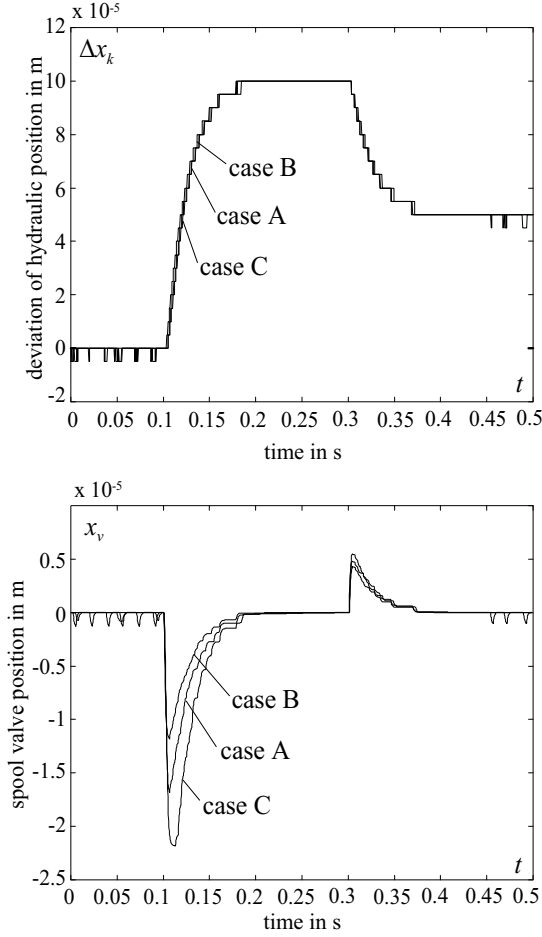


Fig. 9. Simulation results of the position control concept.

1999a; Schlacher *et al.*, 1996; Schlacher and Kugi, 2000), since the design of the spatial distribution of actuators and sensors adds an additional degree of freedom to the design of the control law. Therefore, the controller design has to be considered together with the design of actuators and sensors. Although the sensors and actuators are spatially distributed, the number of control inputs and outputs always remains finite.

Let us remind some results on finite elasticity. The description here is based on a three-dimensional Euclidean space with standard orthonormal basis  $\mathcal{B} = \{\partial_1, \partial_2, \partial_3\}$ , metric  $g = \delta_{ij} dx^i \otimes dx^j$ , and coordinates  $x^i$ ,  $i = 1, 2, 3$ . In the following, the time  $t$  is also denoted by  $t = x^0$ . The symbol  $\otimes$  denotes the tensor product. Now, it is well-known that the dynamical equations of elasticity in this special coordinate system take the form

$$\rho_{\text{Ref}} \partial_0^2 u^i = f^i + d_j (p^{ij}), \quad i = 1, 2, 3. \quad (70)$$

Here  $u = u^i \partial_i$  denotes the displacement of a point  $x$ ,  $\rho_{\text{Ref}}$  is the mass density in the reference configuration,  $d_j$  denotes the total derivative with respect to  $x^j$ ,  $f^i$ 's are the body forces, and  $p$  is the first Piola stress tensor  $p = p^{ij} \partial_i \otimes \partial_j$ . Furthermore, we assume that  $p$  meets the assumption

$$p^{ij} = F_k^i \sigma^{kj}, \quad \sigma^{ij} = \sigma^{ji}, \quad F = (\partial_j u^i + \delta_j^i) \partial_i \otimes dx^j \quad (71)$$

with the second Piola stress tensor  $\sigma = \sigma^{ij} \partial_i \otimes \partial_j$  and the deformation gradient  $F$ . In the case of hyperelasticity, the relations

$$p^{ij} = \rho_{\text{Ref}} \partial_{u^i} W_e, \quad u_j^i = \partial_j u^i \quad (72)$$

with the stored energy function  $W_e(x, F)$  are met additionally. Any function  $W_e$  is not suitable, because  $W_e$  must meet additional conditions concerning the frame indifference and the symmetries of the body (see Gurtin, 1981). If the body force can be derived from a potential  $W_f$ ,

$$f^i = \rho_{\text{Ref}} \partial_{u^i} W_f, \quad (73)$$

then (70) can be put into a Lagrangian form with the Lagrangian

$$L = \int_{\mathcal{B}} \left( \frac{1}{2} \|\partial_0 u\|^2 - W \right) \rho_{\text{Ref}} dx^1 dx^2 dx^3 \quad (74)$$

with  $W = W_e + W_f$  because of (71)–(73). The integral is taken over the reference configuration  $\mathcal{B}$  of the elastic body. Therefore, the next part is concerned with an introduction to infinite-dimensional Lagrangian systems.

In the case of piezoelectricity, the potential (73) must be replaced by a more complex one. Since we deal only with simple structures like beams, we are able to derive this function in the second part under the condition that large deformations but only small strain are taken into account. Based on this assumption, we present solutions for a smart beam in the third part. All stability considerations rely on the simple assumption that a decrease in the total energy implies the stability of the controlled system. The collocation of sensors and actuators is the price which one has to pay, but this can be achieved by special configurations of piezoelectric sensor and actuator layers.

#### 4.1. Lagrange Formalism

Before we consider the action principle in detail, it is advantageous to introduce some useful notation (Olver, 1993). The systems of partial differential equations under consideration involve  $p+1$  independent coordinates denoted by  $(t, x^i) \in X \subset \mathbb{R}^{p+1}$ ,  $i = 1, \dots, p$ , and  $q$  dependent coordinates  $(u^\alpha) \in U \subset \mathbb{R}^q$ ,  $\alpha = 1, \dots, q$ . The total space is the space  $E = X \times U$ . Let us consider a smooth section  $f$  of  $E$ . The  $k$ -th order partial derivatives of  $f$  will be denoted by

$$\frac{\partial^k}{\partial_0^{j_0} \partial_1^{j_1} \dots \partial_p^{j_p}} f = \partial_J f = f_J$$

with  $J = j_0, j_1, \dots, j_p$ , and  $k = \#J = \sum_{i=0}^p j_i$ . Roughly speaking,  $J$  is a multi-index. The  $n$ -th jet space of  $E$  is denoted by  $J^{(n)}E$ , where we use the coordinates  $(t, x^i, u^{(n)})$  with  $u^{(n)} = u_j^\alpha$ ,  $\alpha = 1, \dots, q$ ,  $\#J = 0, \dots, n$ . A smooth section  $f$ ,  $u^\alpha = f^\alpha(t, x)$ , has a unique  $n$ -th prolongation  $u^{(n)} = f^{(n)}(t, x)$  from  $E$  to  $J^{(n)}E$ , which is given by  $u_j^\alpha = \partial_J f^\alpha$ .

Let  $\varphi_\tau$  denote a one-parameter group acting on the variables  $(t, x, u)$  such that the independent variables are not affected or

$$(t, x, \bar{u}) = \varphi_\tau(t, x, u) \quad (75)$$

is met. Then  $\varphi_\tau^{(n)} = \varphi_\tau(t, x, u^{(n)})$  denotes the prolongation of (75) to  $J^{(n)}E$ . Let us consider the Lagrangian functional

$$L = \int_{\mathcal{D}} l(t, x, u^{(n)}) dx \quad (76)$$

with a Lagrangian density well-defined for  $t \geq 0$ . The abbreviation  $dx$  denotes the form  $dx = dx^1 \wedge \dots \wedge dx^p$ , and  $\mathcal{D} \subset \mathbb{R}^p$  stands for a sufficiently nice domain of integration. The action principle states that a solution  $u = f(t, x)$  to the equations of motion of a dynamical system with Lagrangian  $L$  satisfies the condition

$$\begin{aligned} \frac{d}{d\tau} A \Big|_{\tau=0} &= \delta A = 0, \\ A &= \int_{[t_1, t_2] \times \mathcal{D}} l(\varphi_\tau^{(n)}(t, x, f^{(n)})) dx \wedge dt \end{aligned} \quad (77)$$

for any group  $(t, x, u) = \varphi_\tau(t, x, u)$  with  $\varphi_\tau = i$  for  $t \in \{t_1, t_2\}$ . Furthermore,  $A$  is called the action integral (Frankel, 1997). Let  $v \in \mathcal{T}E$  be the infinitesimal generator of  $\varphi$  or

$$v = v^\alpha \partial_{u^\alpha}, \quad v^\alpha = \frac{d}{d\tau} \varphi_\tau^\alpha, \quad v^\alpha = 0 \quad \text{for } t \in \{t_1, t_2\}.$$

Then its prolongation to  $\mathcal{T}J^{(n)}E$  is given by

$$v^{(n)} = v^\alpha \partial_{u^\alpha} + d_J v^\alpha \partial_{u_j^\alpha}, \quad (78)$$

where

$$d_i = \partial_i + u_{J+1_i}^\alpha \partial_{u_j^\alpha} \quad (79)$$

denotes the unique vector field that meets the condition

$$\partial_i v^\alpha(t, x, f^{(n)}(t, x)) = d_i v^\alpha(t, x, u^{(n)}) \Big|_{u^{(n)}=f^{(n)}}.$$

Here, the abbreviations  $J+1_i = j_0, \dots, j_i+1, \dots, j_p$  as well as  $d_J = d_0^{j_0} d_1^{j_1} \dots d_p^{j_p}$  have been used. From

$$\delta A = \int_{[t_1, t_2] \times \mathcal{D}} v^{(n)}(l dx \wedge dt)$$

and the application of the integration-by-parts formula, it follows that

$$\frac{d}{d\tau} A = \int_{[t_1, t_2] \times \mathcal{D}} v^\alpha \delta_\alpha l \, dx \wedge dt + d\omega,$$

where  $\delta_\alpha$  denotes the variational derivative or the Euler-Lagrange operator

$$\delta_\alpha = (-1)^{\#J} d_J \partial_{u_J^\alpha}. \quad (80)$$

Imposing boundary conditions such that the term  $d\omega$  vanishes on  $[t_1, t_2] \times \partial\mathcal{D}$ , we see that the equations of motion are given by

$$\delta_\alpha l(t, x, u^{(n)}) = 0. \quad (81)$$

Now we present a very simplified version of Noether's theorem (Olver, 1993). Applying the special field  $d_0 = \partial_0 + u_{j+1_0}^\alpha \partial_{u_j^\alpha}$  to  $l dx \wedge dt$ , we obtain the identity

$$d_0(l dx \wedge dt) = (\partial_0 l + d_0(e + l)) dx \wedge dt + \left( u_{1, j_1, \dots, j_p}^\alpha \delta_\alpha l \right) dx \wedge dt + d\omega,$$

$$e = \sum_J \sum_{k=1}^{j_0} u_{k, j_1, \dots, j_p}^\alpha (-d_0)^{j_0-k} \partial_{u_J^\alpha} l - l.$$

Now,  $d\omega$  vanishes on the boundary because the imposed boundary conditions and  $\delta_\alpha l = 0$  are met for any solution of (81). Therefore, we get

$$\int_{\mathcal{D}} (e + \partial_0 l) dx = 0 \quad (82)$$

and

$$E = \int_{\mathcal{D}} e dx \quad (83)$$

as a constant of motion, whenever

$$\partial_0 l = 0 \quad (84)$$

is fulfilled. Of course,  $E$  is the total energy of the system, and (82) together with (84) is nothing else than the principle of conservation of energy for time-invariant Lagrangian systems.

Finally, consider the time-varying case with the special Lagrangian density  $l$ ,

$$l = l_0 + l^j U_j, \quad \partial_{u_{j+1_0}^\alpha} l^j = 0,$$

$$\partial_0 l^0 = \partial_0 l^j = 0,$$

and arbitrary functions  $U_j = U_j(t)$ ,  $j = 1, \dots, m$ . From the identity (82) we get

$$\begin{aligned} \int_{\mathcal{D}} d_0 (l_0 + l^j U_j) dx &= \int_{\mathcal{D}} l^j \partial_0 U_j dx, \\ \int_{\mathcal{D}} d_0 (l_0) dx &= -U_j \int_{\mathcal{D}} d_0 l^j dx, \\ - \int_{\mathcal{D}} d_0 (e_0) &= -U_j \int_{\mathcal{D}} d_0 l^j dx, \end{aligned}$$

and derive directly the relation

$$\frac{d}{dt} E_0 = U_j \frac{d}{dt} Y^j, \quad Y^j = \int_{\mathcal{D}} l^j dx, \quad (85)$$

where  $E_0$  denotes the energy of the free system with Lagrangian density  $l^0$  and  $d/dt$  being the time derivative taken along a solution to (81). A natural choice for the output of a system of this type is  $Y^j$ ,  $j = 1, \dots, m$ , since  $U_j dY^j/dt$  is nothing else than the flow of power caused by the input  $U_j$ .

#### 4.2. Piezoelectric Actuators and Sensors

The design of piezoelectric sensors and actuators is based on fundamental relations of linear piezoelectricity. Again, we use the three-dimensional Euclidean space with standard orthonormal basis  $\mathcal{B} = \{\partial_1, \partial_2, \partial_3\}$  and metric  $g = \delta_{ij} dx^i \otimes dx^j$  to describe the constitutive relations. Furthermore, we require that the strain tensor  $\varepsilon = \varepsilon_{ij} dx^i \otimes dx^j$ ,

$$\varepsilon_{ij} = F_i^k g_{kl} F_j^l - \delta_{ij}, \quad (86)$$

remains small, or we have  $|\varepsilon_{ij}| \ll 1$ . We use the bar symbol to indicate the linearized quantity. This assumption allows us to identify the linearized first and second Piola stress tensors or  $\bar{p} \approx \bar{\sigma}$  (see (71)), and to set  $2\bar{\varepsilon}_{ij} = (u_j^i + u_i^j)$ . Neglecting temperature effects, we may write for the constitutive relations of piezoelectricity

$$\bar{\sigma}^{ij} = c^{ijkl} \bar{\varepsilon}_{kl} - a_k^{ij} D^k, \quad (87)$$

$$E_i = -a_i^{kl} \bar{\varepsilon}_{kl} + d_k^i D^k. \quad (88)$$

Here  $D$  denotes the electric flux density and  $E$  stands for the electric field strength (Nowacki, 1975). Equation (87) describes the indirect, and (88) the direct piezoelectric effect. From the assumption concerning  $\sigma$  (71) and the definition of  $\varepsilon$  (see (86)), it follows that  $c^{ijkl} = c^{jikl} = c^{ijlk}$ ,  $a_k^{ij} = a_k^{ji}$  and (72) implies additionally  $c^{ijkl} = c^{klij}$ . Since the free volume charge density is zero inside the piezoelectric lamina and we confine our considerations to the quasi-static case with respect to Maxwell's equations, we get the additional field equations

$$\partial_i D^i = 0, \quad E_i = \partial_i P \quad (89)$$

for  $D$  and  $E$  with electric potential  $P$ .

Piezoelectric actuators have a structure which is highly different with respect to the spatial dimensions. They are usually plates or beams consisting of several piezoelectric layers which are covered by metallic electrodes where a voltage is applied. Although it is possible to derive the stored energy function  $W_e(x, F)$  (cf. (72)) from the relations (87), (89) for the linearized scenario (see, e.g., Kugi *et al.*, 1999a; Schlacher *et al.*, 1996), we pursue another, more axiomatic approach here. For the sake of simplicity, we restrict our considerations to the beams which are considered as one-dimensional structures moving in a two-dimensional Euclidean space with standard metric  $g$ . Let

$$x^1 = \varphi^1(S, t), \quad x^2 = \varphi^2(S, t) \quad (90)$$

describe the position of an idealized beam such that  $S$  is the arc length of the beam at the reference position given by  $x^1 = S = \varphi^1(S, 0)$ ,  $x^2 = 0 = \varphi^2(S, 0)$  for  $0 \leq S \leq L$ . The independent variables are  $t$  and  $S$ , while the dependent ones are  $u^1$  and  $u^2$  with  $\varphi^1 = x^1 + u^1$ ,  $\varphi^2 = x^2 + u^2$ . Now, it is well-known that the arc-length and the curvature of  $\varphi(S, t)$  determine the position unambiguously up to a rotation. Furthermore, let us assume that the energy can be stored only by stretching or bending. Then we may set

$$W_e = W_{e,m}(S, \varepsilon_m, \kappa_m, U) \quad (91)$$

with

$$(1 + \varepsilon_m)^2 = \varphi^*(g) = (\varphi_{0,1}^1)^2 + (\varphi_{0,1}^2)^2, \quad (92)$$

where  $U$  denotes the voltages applied to the different layers. Furthermore, we get the additional relations

$$\partial_S s = 1 + \varepsilon_m, \quad (93)$$

$$\partial_S \alpha = \kappa_m (1 + \varepsilon_m),$$

$$\begin{bmatrix} 1 + u_{0,1}^1 \\ u_{0,1}^2 \end{bmatrix} = (1 + \varepsilon_m) \begin{bmatrix} \cos(\alpha) \\ \sin(\alpha) \end{bmatrix}, \quad (94)$$

with the angle  $\alpha$  between  $\varphi_{0,1}(S, 0)$  and  $\varphi_{0,1}(S, t)$ . To get a further simplification, we assume that such a device is built up symmetrically with respect to the mid-plane and that the different piezoelectric and structural layers are perfectly bonded to the substrate. Although we assume symmetry with respect to the mid-plane, we can apply the voltage  $U_i$  of the layer  $i$  symmetrically or anti-symmetrically with respect to this plane. A choice for the function  $W_e$  that meets all the requirements presented above is given by

$$\begin{aligned} \int_L \rho_{\text{Ref}} W_{e,m} dS &= \int_L \frac{\rho_{\text{Ref}}}{2} (k_\varepsilon \varepsilon_m^2 + k_\kappa \kappa_m^2) dS - \sum_{\alpha=1}^{n_A} U_\alpha^A L_A^\alpha - \sum_{\beta=1}^{n_B} U_\beta^B L_B^\beta, \\ L_A^\alpha &= \int_L \rho_{\text{Ref}} \mu_A^\alpha(S) \varepsilon_m dS, \\ L_B^\beta &= \int_B \rho_{\text{Ref}} \mu_B^\beta(S) \kappa_m dS. \end{aligned} \quad (95)$$

The index  $A$  denotes couples of layers with symmetrically applied voltages and the index  $B$  corresponds to the couples where the voltages are applied anti-symmetrically. The functions  $\mu_A^\alpha(S)$  and  $\mu_B^\beta(S)$  depend on the special form of the electrodes and/or the piezoelectric laminates. They will be designed later depending on the requirements of the control problem. The following facts are worth mentioning. If one simplifies the new stored energy function with respect to the small strain assumptions, then this simplified function is derivable by classical beam theory based on the relations (86)–(89), see, e.g., (Kugi, 2000; Schlacher *et al.*, 1996). Within this small strain scenario, the function  $\varphi(S, t)$  describes the movement of a coordinate line and does not describe the movement of the physical mid-line in general. Figure 10 sketches a possibility of creating a specified spatial distribution,  $\mu_A^\alpha(S)$  and  $\mu_B^\beta(S)$ , by means of shaping the corresponding electrodes. At this point it should be explained that the poling direction in the piezoelectric layer can only be up or down, due to polarity. The voltage supplied,  $U_\alpha^A$  or  $U_\beta^B$ , is either positive or negative. Figure 10 shows all of the different possible combinations for creating a symmetrically or an anti-symmetrically supplied piezoelectric layer couple. Figure 11 shows another possibility, where the thickness of the piezoelectric lamina varies over the length of the layer. Of course, a combination of these methods is also possible. It should be emphasized that Figs. 10 and 11 depict only the ideas relating to the design of a specified shaping function (Kugi *et al.*, 1999a). In a practical application, one will use more sophisticated surface patterns of the electrodes for achieving the shaping functions (see, e.g., (Lee and Moon, 1990) and the references cited therein).

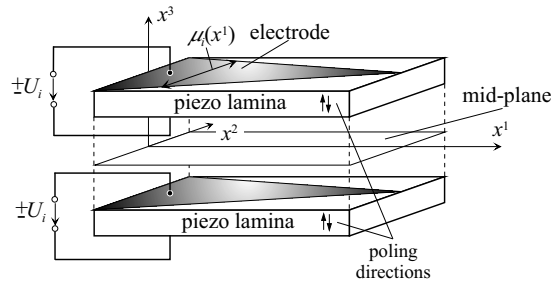


Fig. 10. Principle of surface shaping of the electrode for an actuator layer couple.

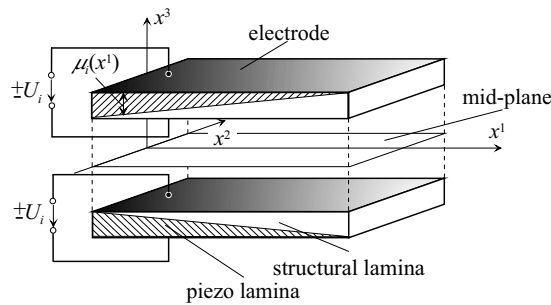


Fig. 11. Principle of shaping the piezoelectric lamina for an actuator layer couple.

The design of piezoelectric sensors follows a procedure similar to the one applied to the actuators. The corresponding electrodes of a layer are short circuited. Within the small-strain scenario, the derivation of the sensor equations is based on the relations (86), (88), (89). The output of such a sensor is the charge  $Q$  of the capacity built up by the electrodes and the piezoelectric laminate. Again, we assume the symmetry of the device with respect to the mid-plane and we can take the sum or the difference of the corresponding charges. The analysis of the modeling problem yields

$$\begin{aligned} Y_A &= \int_L \lambda_A(S) \varepsilon_m \rho_{\text{Ref}} dS, \\ Y_B &= \int_L \lambda_B(S) \kappa_m \rho_{\text{Ref}} dS, \end{aligned} \quad (96)$$

where the index  $A$  denotes the couples of layers with the sum of the charges and the index  $B$  corresponds to the couples where the difference is taken. Again, the functions  $\lambda_A(S)$  and  $\lambda_B(S)$  depend on the special construction of the layers, and they can be designed with respect to the control problem. The principle of shaping the sensor layers is shown in Fig. 12, see (Kugi *et al.*, 1999a). Here the right choice of the polarization profile within each layer of one sensor layer couple offers an additional possibility to create the shaping functions  $\lambda_A(S)$  and  $\lambda_B(S)$  too.

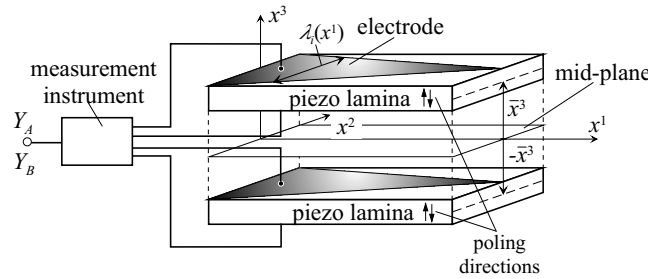


Fig. 12. Principle of surface shaping of the electrode for a sensor layer couple.

If we compare (95) and (96), then it can be seen that this design allows us to collocate the actuators and sensors in a straightforward manner.

### 4.3. Design of a Smart Beam

Let us consider the cantilever beam of Fig. 13 moving in a two-dimensional Euclidean space with standard orthonormal basis  $\mathcal{B}$ . Again, the independent coordinates are  $t$ ,  $S = x^1$  and the dependent coordinates are the displacements  $u^j$ ,  $j = 1, 2$ .  $L$  denotes the length of the beam in the reference configuration with  $u^1 = u^2 = 0$  for  $S \in [0, L]$ . Furthermore, we assume that the line mass density  $\rho_{\text{Ref}}$  is constant in this configuration. The beam is equipped with several piezoelectric actuator layers to counteract the gravity with acceleration  $g$  and several sensor layers to supply the control system with the required measurements. The design of the spatial distributions

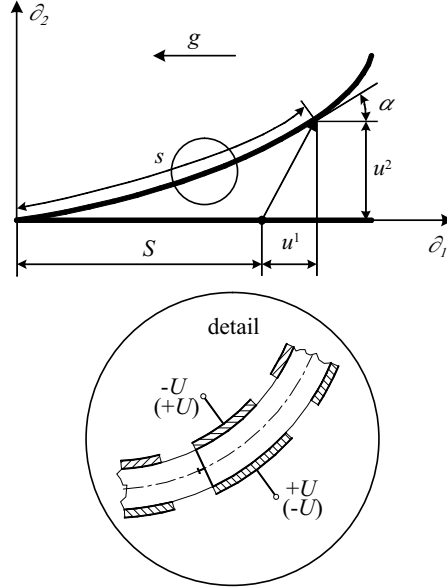


Fig. 13. The considered smart beam.

of these layers is part of the controller design itself. The map from the reference configuration to the current one is again denoted by  $\varphi$  (cf. (90)). The derivation of the evolutionary equations of the smart beam is based on the conservation of mass and on the balance laws of momentum, as well as those of moment of momentum (Marsden and Hughes, 1994). Furthermore, we neglect the rotational inertia. According to these assumptions, we get the kinetic energy density  $W_k$ ,

$$W_k = \frac{\rho_{\text{Ref}}}{2} \left( (u_{1,0}^1)^2 + (u_{1,0}^2)^2 \right). \quad (97)$$

The effect of gravity, which acts like a body force on the beam, is taken into account by the potential

$$W_f = g \rho_{\text{Ref}} u^1 \quad (98)$$

and the stored energy function  $W_{e,m}$  of the beam with piezoelectric layers is given by (95). According to (74), one gets the Lagrangian

$$L = \int_L (W_k - W_{e,m} - W_f) dS. \quad (99)$$

To complete the problem, we have to add the kinematic boundary conditions which are in this case given by

$$u(0, t) = 0 \quad \text{and} \quad \alpha(0, t) = 0,$$

see Fig. 13. The dynamic boundary conditions follow directly from the Lagrange formalism.

Now we are able to formulate the design problem: Find a control law with suitable actuators and sensors such that the reference position is stabilized and such that the influence of the gravity is eliminated at least in this position. The controller design takes place in two steps. In the first step, we change the potential energy function such that its global minimum occurs at the required position. In the second step, we inject damping to achieve asymptotic stability (see, e.g., (Schlacher, 1998)). Furthermore, we have to distinguish two cases. If the beam is stiff enough such that there exists only one equilibrium (of course, with  $\alpha = 0$ ), then we skip the following step. Otherwise, we choose the control laws

$$U_j^B = -k_B L_B^j, \quad j = 1, \dots, m$$

and the actuators (cf. (95)) with

$$\mu_B^j = \begin{cases} 1 & \text{if } S \in [S^j, S^j + \Delta S], \\ 0 & \text{otherwise,} \end{cases}$$

and  $0 \leq S^1$ ,  $S^j + \Delta S < S^{j+1}$ ,  $j = 1, \dots, m-1$ ,  $S^m + \Delta S \leq L$ ,  $\Delta S > 0$  of the type

$$L_B^j = \int_L \mu_B^j \rho_{\text{Ref}} \kappa_m \, dS = \rho_{\text{Ref}} \Delta \alpha^j, \quad (100)$$

$$\Delta \alpha^j = \alpha(S^j + \Delta S) - \alpha(S^j), \quad \mu_B^j = 1.$$

Let  $s$  denote the arc length at the actual position. Then (100) follows from (93) and  $\partial_s \alpha = \kappa_m$ . These actuators can be realized with patches of piezoelectric layers in a straightforward manner. In addition, this type of control law is derivable from the potential

$$W_U^j = \frac{k_B}{2} (L_B^j)^2$$

because of

$$\delta_\alpha \left( \frac{k_B}{2} (L_B^j)^2 \right) = \underbrace{k_B L_B^j}_{-U_j^B} \int_L \delta_\alpha \left( \mu_B^j \rho_{\text{Ref}} \kappa_m \right) \, dS$$

and  $\delta_\alpha$  of (80). For a sufficiently large  $k_B > 0$  and a sufficient number of patches, we can always obtain that there exists only one equilibrium with  $\alpha = 0$ .

To get a closer insight into the influence of the gravity on the beam, we rewrite the form  $W_f/g\rho_{\text{Ref}}$  (cf. (98)) as

$$\begin{aligned} u^1 &= d_S ((S-L)u^1) + (L-S)u_{0,1}^1 \\ &= (L-S)((\varepsilon_m+1)\cos\alpha-1) + d_S ((S-L)u^1) \end{aligned}$$

because of (94). Since the first term on the right-hand side vanishes on the boundary  $S \in \{0, L\}$ , it is easy to see that the control law  $U^A = -g$  with the actuator (95)

$$L_A = \int_L (L-S) \varepsilon_m \rho_{\text{Ref}} \, dS \quad (101)$$

cancels the influence of the gravity on the beam at the equilibrium  $\alpha = 0$ . The collocated sensors for the actuators (100) and (101) follow directly from (96) as  $Y_B^j = L_B^j$  and  $Y_A = L_A$ .

According to this construction, the global minimum  $W_{\min}$  of the function  $W = W_f + W_{e,m}$  occurs at  $\alpha = 0$ ,  $\varepsilon = 0$ . To finish the controller design, we have to add damping to the system. According to the previous results, we choose the control laws

$$U_j^B = -k_B Y_B^j - d_B \frac{d}{dt} Y_B^j,$$

$$U_A = -g Y_A - d_A \frac{d}{dt} Y_A,$$

where  $d_A > 0$ ,  $d_B > 0$ .

Finally, the set of evolutionary equations of the closed loop in Lagrangian form can be derived from the potential presented above. The Euler-Lagrange operators are given by (80) for  $\#J = 2$ . It is worth deriving these equations using a computer algebra program due to the enormous complexity of this set of equations. Of course, we can only show that

$$\frac{d}{dt} E^0 = -d_A \left( \frac{d}{dt} Y_A \right)^2 - d_B \sum_{j=1}^m \left( \frac{d}{dt} Y_B^j \right)^2 \leq 0$$

is met for the proposed controllers (see (85)). Asymptotic stability cannot be proven here, but it follows from the insight into the physics of the smart beam. It is worth mentioning that, although the piezoelectric beam is an infinite-dimensional dynamical system, the control law uses a finite number of sensors and actuators only.

## 5. Conclusions

This contribution is concerned with different control strategies for mechatronic systems. The physical nature of the plants to be controlled in combination with a strong mathematical formulation based on differential geometry and differential algebra serve as a common basis for the controller design. Moreover, for the control concepts to be practically feasible some special features and restrictions of the plants have to be taken into account already within the control synthesis task. Thus, for example, in most of the control applications only some state variables are measurable, the signals are corrupted by transducer and quantization noise, the sensors and actuators have a limited accuracy, and some parameters are only known inaccurately or are even varying slowly due to, e.g., aging processes. Furthermore, it turns out that by an appropriate design of actuators and sensors the control problem itself can be drastically simplified. Of course, this paper does not intend to give a general solution to all these problems. But by means of three different applications, namely a PWM-controlled dc-to-dc converter, the hydraulic gap control in steel rolling, and an infinite-dimensional smart beam structure, it is shown how control theory can be used to solve the control design problem by considering special features of the plant and, what is even more

challenging, how an interdisciplinary design can improve the existing products and is able to lead to new ones.

## References

- Fleck N.A., Johnson K.L., Mear M.E. and Zhang L.C. (1992): *Cold rolling of foil*. — Proc. Instn. Mech. Engrs., Part B: J. Engineering Manufacture, Vol.206, pp.119–131.
- Frankel T. (1997): *The Geometry of Physics*. — Cambridge: Cambridge University Press.
- Gurtin M. (1981): *Topics in Finite Elasticity*. — CBMS/NSF Conf. Series 35, SIAM, Philadelphia.
- Hensel A. and Spittel T. (1990): *Kraft- und Arbeitsbedarf bildsamer Formgebungsverfahren*. — Leipzig: Deutscher Verlag für Grundstoffindustrie.
- Isidori A. (1996): *Nonlinear Control Systems*. — London: Springer.
- Isidori A. and Astolfi A. (1992): *Disturbance attenuation and  $H_\infty$ -control via measurement feedback in nonlinear systems*. — IEEE Trans. Automat. Contr., Vol.37, No.9, pp.1283–1293.
- Kassakian J.G., Schlecht M.F., Verghese G.C. (1992): *Principles of Power Electronics*. — New York: Addison Wesley.
- Khalil H.K. (1992): *Nonlinear Systems*. — New York: Macmillan Publishing Company.
- Knobloch H.W., Isidori A. and Flockerzi D. (1993): *Topics in Control Theory*. — DMV Seminar Band 22, Bases: Birkhäuser.
- Kugi A. (2000): *Non-linear Control Based on Physical Models*. — Lecture Notes in Control and Information Sciences 260, London: Springer.
- Kugi A. and Schlacher K. (1999): *Nonlinear  $H_\infty$ -controller design for a DC-to-DC power converter*. — IEEE Trans. Contr. Syst. Techn., Vol.7, No.2, pp.230–237.
- Kugi A., Schlacher K. and Irschik H. (1999a): *Infinite dimensional control of nonlinear beam vibrations by piezoelectric actuator and sensor layers*. — Nonlin. Dynam., Vol.66, pp.267–269.
- Kugi A., Schlacher K. and Keintzel G. (1999b): *Position Control and Active Eccentricity Compensation in Rolling Mills*. — Automatisierungstechnik, Oldenbourg, Vol.47, No.8, pp.342–349.
- Lee C.-K. and Moon F.C. (1990): *Modal sensors/actuators*. — J. Appl. Mech., Trans. ASME, Vol.57, pp.434–441.
- Marsden J.E. and Hughes T.J. (1994): *Mathematical Foundations of Elasticity*. — New York: Dover Publications.
- Merritt H.E. (1967): *Hydraulic Control Systems*. — New York: Wiley.
- Mohan N., Undeland T.M. and Robbins W.P. (1989): *Power Electronics: Converters, Applications, and Design*. — New York: Wiley.
- Nijmeijer H. and van der Schaft A.J. (1991): *Nonlinear Dynamical Control Systems*. — New York: Springer.

- Nowacki W. (1975): *Dynamic Problems of Thermoelasticity*. — Warsaw: Noordhoff Int. Publishing, PWN-Polish Scientific Publishers.
- Olver P.J. (1993): *Applications of Lie Groups to Differential Equations*. — New York: Springer.
- Sastry S. (1999): *Nonlinear Systems*. — New York: Springer.
- Schlacher K. (1998): *Mathematical strategies common to mechanics and control*. — Zeitschrift für angewandte Mathematik und Mechanik, ZAMM, No.78, pp.723–730.
- Schlacher K. and Kugi A. (2000): *Control of mechanical structures by piezoelectric actuators and sensors*, In: Stability and Stabilization of Nonlinear Systems (Aeyels D., Lamnabhi-Lagarrigue F., van der Schaft A., Eds.). — London: Springer, pp.275–292.
- Schlacher K., Irschik H. and Kugi A. (1996): *Control of nonlinear beam vibrations by multiple piezoelectric layers*, In: Proc. IUTAM Symp. *Interaction between Dynamics and Control in Advanced Mechanical Systems* (van Campen D.H., Ed.). — Dordrecht: Kluwer, pp.355–363.
- Sira Ramírez H. (1989): *A geometric approach to pulse-width modulated control in nonlinear dynamical systems*. — IEEE Trans. Automat. Contr., Vol.34, No.2, pp.184–187.
- Tzou H.S. (1992): *Active piezoelectric shell continua*, In: Intelligent Structural Systems (Tzou H.S. and Anderson G.L., Eds.). — Dordrecht: Kluwer, pp.9–74.
- van der Schaft A.J. (1993): *Nonlinear state space  $H_\infty$  control theory*, In: Essays on Control: Perspectives in the Theory and its Applications (Trentelman H.L. and Willems J.C., Eds.). — Boston: Birkhäuser, pp.153–190.
- van der Schaft A.J. (2000):  *$L_2$ -Gain and Passivity Techniques in Nonlinear Control*. — London: Springer.